BRAIN CONNECTIVITY
Volume 9, Number 1, 2019

DOI: 10.1089/brain.2018.0579

Transient Patterns of Functional Dysconnectivity in Clinical High Risk and Early Illness Schizophrenia Individuals Compared with Healthy Controls

Eva Mennigen,[1,2,*] Susanna L. Fryer,[3,4] Barnaly Rashid,[1] Eswar Damaraju,[1] Yuhui Du,[1,5] Rachel L. Loewy,[3] Barbara K. Stuart,[3] Vince D. Calhoun,[1,2,†] and Daniel H. Mathalon[3,4,†]

Abstract

Schizophrenia shows abnormal dynamic functional network connectivity (dFNC), but it is unclear whether these abnormalities are present early in the illness course or precede illness onset in individuals at clinical high risk (CHR) for psychosis. We examined dFNC from resting-state functional magnetic resonance imaging data in CHR ($n = 53$), early illness schizophrenia (ESZ; $n = 58$), and healthy control (HC; $n = 70$) individuals. We applied a sliding temporal window approach capturing five distinct dFNC states. In ESZ patients, the likelihood of transitioning from state 4, a state that exhibited greater cortical–subcortical hyperconnectivity and also lacked typically observed anticorrelation between the default mode network and other functional networks, to a hypoconnected state was increased compared with HC and CHR groups. Furthermore, we investigated the interaction of group and state on dFNC. Overall, HC individuals showed significant changes of connectivity between states that were absent or altered in ESZ patients and CHR individuals. Connectivity differences between groups were identified primarily in two out of the five states, in particular, between HC and ESZ groups. In summary, it appears that the interaction effect was mostly driven by (1) dynamic connectivity changes in HC that were abnormal in CHR and ESZ individuals and (2) the fact that dysconnectivity between groups was only present in some states. These findings underscore the likelihood that abnormalities are present not only in static FNC but also in dFNC, in individuals at CHR for schizophrenia.

Keywords: clinical high risk; dysconnectivity; independent component analysis; schizophrenia

Introduction

Before the onset of psychosis, most patients with schizophrenia and other psychotic disorders exhibit a prodromal syndrome for several years typically characterized by (1) attenuated psychotic symptoms, or less often, brief intermittent psychotic symptoms and (2) a decline in social and occupational functioning (Fusar-Poli et al., 2013; Phillips et al., 2005). Functional dysconnectivity has been theorized to underlie psychotic symptoms, such as delusions and hallucinations, because it might disrupt the integration of information from segregated brain areas (Adams et al., 2013; Calhoun et al., 2009; Rubinov and Bullmore, 2013). With the development of validated clinical criteria for identifying individuals at clinical high risk (CHR) for psychosis, we are also in a position to ask whether dysconnectivity is present during this period.

Resting-state functional magnetic resonance imaging (rs-fMRI) has proven to be a useful tool to analyze functional network connectivity (FNC), for example, based on group independent component analysis (GICA) (Calhoun et al., 2001; McKeown et al., 1998). As a special case of blind source separation, GICA identifies maximally (spatially) independent components across the brain with correlated time courses. Furthermore, unlike seed-based connectivity analyses where one anatomical region of interest is chosen and time courses from

[1]The Mind Research Network, Albuquerque, New Mexico.
[2]Department of Electrical and Computer Engineering, University of New Mexico, Albuquerque, New Mexico.
[3]Department of Psychiatry, University of California, San Francisco, California.
[4]Mental Health Service, San Francisco VA Medical Center, San Francisco, California.
[5]School of Computer & Information Technology, Shanxi University, Taiyuan, China.
Current affiliation: Department of Psychiatry and Biobehavioral Sciences, University of California, Los Angeles, California.
†Equally contributing senior authors.

this seed and all other voxels in the brain are correlated, GICA is a fully data-driven approach that does not make *a priori* assumptions about which brain regions are most important to interrogate (Fox et al., 2005). Independent components identified by GICA can be divided into noise-related components and meaningful intrinsic connectivity networks (ICNs) that reflect coherently fluctuating anatomical regions with respect to their time courses. Functional domains can be assembled by grouping respective ICNs. In this study, eight functional domains are investigated, that is, subcortical (SC), salience (SAL), auditory (AUD), sensory-motor, visual (VIS), cognitive control (CC), default mode network (DMN), and cerebellar domains, to capture whole brain connectivity. FNC within and between functional domains can be estimated by correlating time courses of ICNs. The most common way to investigate FNC is to analyze rs-fMRI data pooled across the duration of the scan as one cross-correlation matrix of time courses of all identified ICNs, that is, static FNC.

Applying this very technique, it has been shown that patients with schizophrenia exhibit hyperconnectivity between the DMN and prefrontal task-positive brain areas and hypoconnectivity within the DMN compared with healthy controls (HCs) (Arbabshirani et al., 2013; Camchong et al., 2011; Jafri et al., 2008; Manoliu et al., 2014). With respect to CHR individuals, Du and colleagues (2017b) showed that hypoconnectivity is present within different functional domains, among them the SAL, fronto-occipital- and fronto-occipito-parietal-networks, and the DMN. In this study, Du and colleagues (2017b) also showed that dysconnectivity was more pronounced in patients with early illness schizophrenia (ESZ) after diagnosis (mean illness duration 2.09 years) compared with dysconnectivity observed in CHR individuals. These findings are bolstered up by findings from seed-based connectivity analyses. Results of these studies converge in showing CHR individuals to lack the usually observed anticorrelation of time courses between the DMN and task-related prefrontal brain areas (Shim et al., 2010). Furthermore, static connectivity analyses using a thalamic seed, including a report based on the data analyzed in this study (Ferri et al., 2017), have shown thalamocortical hyperconnectivity with somatosensory (Anticevic et al., 2015) and AUD domains (Ferri et al., 2017) and reduced connectivity with the cerebellum (CB) and anterior cingulate cortex (Anticevic et al., 2015; Ferri et al., 2017), which predicts subsequent transition to full-blown psychosis (Anticevic et al., 2015). Furthermore, Wotruba and associates (2013) observed positive symptom severity in CHR individuals to be directly correlated with connectivity strength between the right anterior insula, an area associated with the SAL network, and the posterior cingulate cortex, a node of the DMN.

However, it has been shown that functional connectivity is not static over the entire time of typical rs-fMRI protocols (e.g., 5 min); rather, connectivity patterns vary over relatively shorter time scales of seconds to minutes, motivating the development of a dynamic approach for the assessment of connectivity between ICNs, that is, dynamic FNC (dFNC), which yields more temporally fine-grained results (Allen et al., 2012; Calhoun et al., 2014; Damaraju et al., 2014; Rashid et al., 2014). As we know from task-based fMRI studies, the dynamic reconfiguration of functional connectivity plays an important role in cognitive processes, which highlights the importance of evaluating dFNC in disorders accompanied by impaired cognitive functioning (Shine et al., 2016; Vatansever et al., 2015). This dynamic approach evaluates FNC with sliding temporal windows, allowing the identification of multiple discrete connectivity states occurring during the resting-state scan as well as characterizing connectivity behavior based on dynamic indices such as mean dwell time (MDT, time spent in a specific state before transitioning to another state), frequency (time spent in a specific state across the entire scan time), and the absolute number of transitions (NTs). It has been shown that the dynamic states identified with this approach are recurring and reproducible across different samples and studies (Abrol et al., 2017) and also that dFNC changes are associated with changes in various electro-encephalography measures (Allen et al., 2017).

Following the same methodological approach as in this article, Damaraju and associates (2014) showed in their dFNC analysis that patients with chronic schizophrenia spend more time in ''loosely connected'' states, that is, states that show lower whole-brain connectivity between functional domains. Moreover, dysconnectivity in schizophrenia was more pronounced in states that exhibit antagonism, that is, anticorrelation, between cortical and SC regions.

Recently, Du and colleagues applied a new method of functional connectivity analysis called group information guided ICA (GIG-ICA) (Du and Fan, 2013; Du et al., 2017c) to the same data analyzed in this article (Du et al., 2017a). In this approach, ICA is applied to windowed FNC matrices derived from time courses from atlas-based region of interests, yielding one group-wise *dominant* connectivity state. Here, dominance refers to the highest contribution to variance of dynamic connectivity. These dominant states can then be further investigated. With regard to the current sample, Du and associates (2017a) found that CHR individuals and ESZ patients exhibit dysconnectivity in cerebellar, temporal, thalamic, and prefrontal brain areas in the dominant group state. Again, CHR individuals exhibited less severely altered connectivity compared with patients with schizophrenia (Du et al., 2017a). Since this method focuses rather on identifying one dominant state using a sliding temporal window approach than on identifying multiple distinct states, dFNC in terms of Allen and colleagues (2012) has yet to be examined in the psychosis risk syndrome. In particular, the investigations of (1) indices characterizing dynamism of connectivity and (2) changing patterns of dysconnectivity across distinct states are lacking. We aimed at filling this gap by reanalyzing the same data previously analyzed by Ferri and colleagues (2017) and Du and colleagues (2017a,b) using an established dFNC approach (Allen et al., 2012) that complements the GIG-ICA approach used by Du and colleagues (2017a,b). The approach in this article relies on data-driven estimation of ICNs encompassing the whole brain. Based on these, dynamic characteristics like changes in FNC are being evaluated in the context of multiple dFNC states. The aim of this study was to examine whether aberrant dFNC between brain networks is present early in the course of schizophrenia, and further, whether such abnormalities are evident during the psychosis risk syndrome before the onset of full-blown psychosis.

Materials and Methods

Participants

CHR individuals ($n = 53$) were recruited from University of California, San Francisco (UCSF) early psychosis clinical

Table 1. Demographic Data

	HC (n = 70)		*CHR individuals (n = 53)*		*ESZ patients (n = 58)*	
	Mean	*SD*	*Mean*	*SD*	*Mean*	*SD*
Age (years)	21.9	5.6	20.4	4.5	21.8	3.8
PANSS positive symptoms	—	—	—	—	13.7[a]	4.8
PANSS negative symptoms	—	—	—	—	17.4[a]	6.6
SOPS positive symptoms	—	—	9.14[b]	4.6	—	—
SOPS negative symptoms	—	—	12.2[b]	5.8	—	—
Maximum of absolute translation motion displacement (mm)	0.8	0.6	1.1	1.4	1.2	1.3
Maximum of absolute rotation motion displacement (degrees)	0.8	1.0	1.0	0.9	0.9	0.8
	n	%	n	%	n	%
Male	41	59	32	62	38	65

[a]Indicates $n = 56$ ESZ individuals with valid clinical data.
[b]Indicates $n = 36$ CHR individuals with valid clinical data.
SD, standard deviation; HC, healthy control; CHR, clinical high risk; ESZ, early illness schizophrenia; PANSS, Positive and Negative Syndrome Scale; SOPS, Scale of Prodromal Symptoms.

research program, local clinics, and school counseling centers. The Criteria of Prodromal Syndromes (Miller et al., 2002), as assessed with the Structured Interview for Prodromal Syndromes (McGlashan et al., 2001) administered by a trained interviewer, were used to identify individuals exhibiting one or more of three nonmutually exclusive CHR subsyndromes: Attenuated Psychotic Symptoms (92.5%), Brief Intermittent Psychotic Symptoms (1.9%), and Genetic Risk and Deterioration (7.5%) (Miller et al., 2003).

ESZ patients ($n = 58$) were recruited from the UCSF early psychosis clinical research program and from local community clinics. ESZ patients met DSM-IV criteria for schizophrenia ($n = 63.8\%$), schizoaffective ($n = 27.6\%$), or schizophreniform ($n = 6.9\%$) disorder based on the Structured Clinical Interview for DSM-IV (SCID) (First et al., 2002) administered by a trained interviewer. The mean illness duration for ESZ patients was 2.09 years (standard deviation, 1.37).

Using the Scale of Prodromal Symptoms (SOPS) (Miller et al., 2003) for CHR individuals and the Positive and Negative Syndrome Scale (PANSS) (Kay et al., 1987) for ESZ patients, symptom severity was assessed by trained clinical raters.

HC individuals ($n = 70$) were recruited from the community and did not meet criteria for any Axis I diagnosis based on the SCID. For participants <16 years of age, the Schedule for Affective Disorders and Schizophrenia for School-Age Children (Kiddie-SADS) Present and Lifetime Version (Kaufman et al., 1997) was used to assess for Axis I diagnoses in younger teenagers.

General exclusion criteria included DSM-IV substance dependence in the past year (except nicotine), a history of head

Table 2. Overview of Antipsychotics in Clinical High Risk and Early Illness Schizophrenia Individuals

ESZ antipsychotic	*Number of times prescribed*	*CHR antipsychotics*	*Number of times prescribed*
Aripiprazole	21	Aripiprazole	5
Risperidone	14	Quetiapine	4
Olanzapine	10	Olanzapine	2
Ziprasidone	4	Risperidone	2
Clozapine	4	Ziprasidone	1
Quetiapine	3		14
Haloperidole[a]	2		
Perphenazine[a]	2		
Paliperidone	1		
Thiotixene[a]	1		
	62		
Nine ESZ patients with two APs	N	*Two CHR individuals with two APs*	N
Aripiprazole + Risperidone	3	Aripiprazole + Risperidone	1
Aripiprazole + Olanzapine	2	Quetiapine + Ziprasidone	1
Aripiprazole + Perphenazine	1		
Aripiprazole + Ziprasidone	1		
Paliperidone + Perphenazine	1		
Ziprasidone + Haloperidol	1		

[a]First generation antipsychotics.

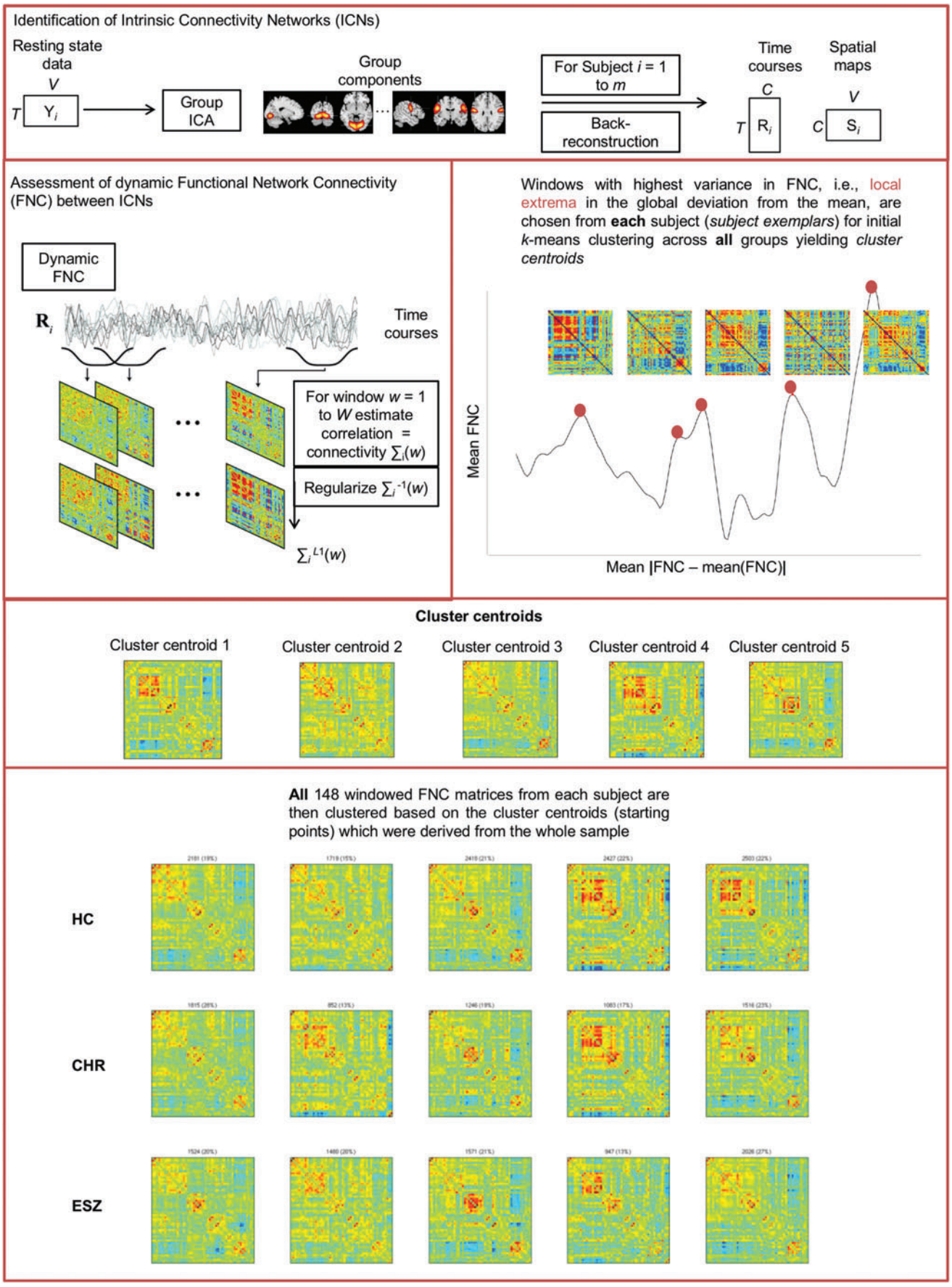

FIG. 1. Dynamic FNC analysis steps and results. FNC, functional network connectivity. Color images are available online.

injury with loss of consciousness, neurological disorders, or a first-degree relative with a psychotic illness (for HC individuals only).

Written informed consent was obtained from participants, or from their parents/legal guardians in the case of minors (who also provided written assent), under protocols approved by the institutional review board at UCSF. Demographic data are presented in Table 1. The final sample comprised 70 HC, 53 CHR, and 58 ESZ individuals, and groups did not differ significantly with regard to age and gender. At the time of fMRI scanning, 12 CHR (22.6%) and 53 ESZ (91.4%) individuals were taking antipsychotic medication; Table 2 gives an overview on antipsychotic medication in both groups.

Data acquisition

rs-fMRI data were collected at the UCSF Neuroimaging Center using a 3T Siemens Trio (Erlangen, Germany) scanner. A total of 180 images were acquired at rest while participants were instructed to keep their eyes closed. The echo planar imaging sequence had the following parameters: 32 axial slices, thickness 3.5 mm, field of view 24 cm, repetition time (TR) 2 sec, echo time 29 msec, and flip angle 75°.

rs-fMRI preprocessing

Preprocessing was conducted using SPM 8 (http://fil.ion.ucl.ac.uk/spm) and the Data Processing Assistant for Resting-State fMRI (DPARSF) toolbox (Yan and Zang, 2010). The first 10 images were discarded due to equilibration effects, leaving 170 images for further analysis. Further preprocessing included slice time correction, realignment to the first volume, spatial normalization to a standard Montreal Neurological Institute template, reslicing to a voxel size of $3\times3\times3$ mm, and smoothing with a 6 mm Gaussian kernel. Individuals included in this study did not exceed 4 mm/4° movement across volumes.

FNC analysis

Group independent component analysis. Figure 1 depicts analysis steps for GICA and for the k-means clustering approach. Spatial GICA (Calhoun and Adali, 2012; Calhoun et al., 2001) decomposes the whole brain rs-fMRI data into linear mixtures of spatially independent components. GICA was performed using the GICA fMRI toolbox (GIFT) (http://mialab.mrn.org/software/gift) with two data reduction steps using principal component analysis: (1) a subject-specific reduction of time points from 170 time points to 120 temporal principle components comprising weighted sums of time points and (2) a group-wise reduction of the concatenated subject-reduced data to 100 components, each consisting of a spatial map and a corresponding time course using the expectation-maximization algorithm (Roweis, 1998). Preprocessing in GIFT included z-scoring of time courses to normalize variance. ICA was repeated 20 times in ICASSO (Himberg and Hyvärinen, 2003) using the infomax algorithm (Bell and Sejnowski, 1995) and the best run was selected (Ma et al., 2011) to ensure stability of estimation. We used spatial–temporal back reconstruction (Calhoun et al., 2001; Erhardt et al., 2011) to estimate subject-specific time courses and spatial maps for each independent component. The resulting 100 independent components were manually reviewed to identify meaningful ICNs based on the automated anatomic labeling atlas (Tzourio-Mazoyer et al., 2002). ICNs were evaluated to confirm that peak locations were located in gray matter; showed minimal overlap

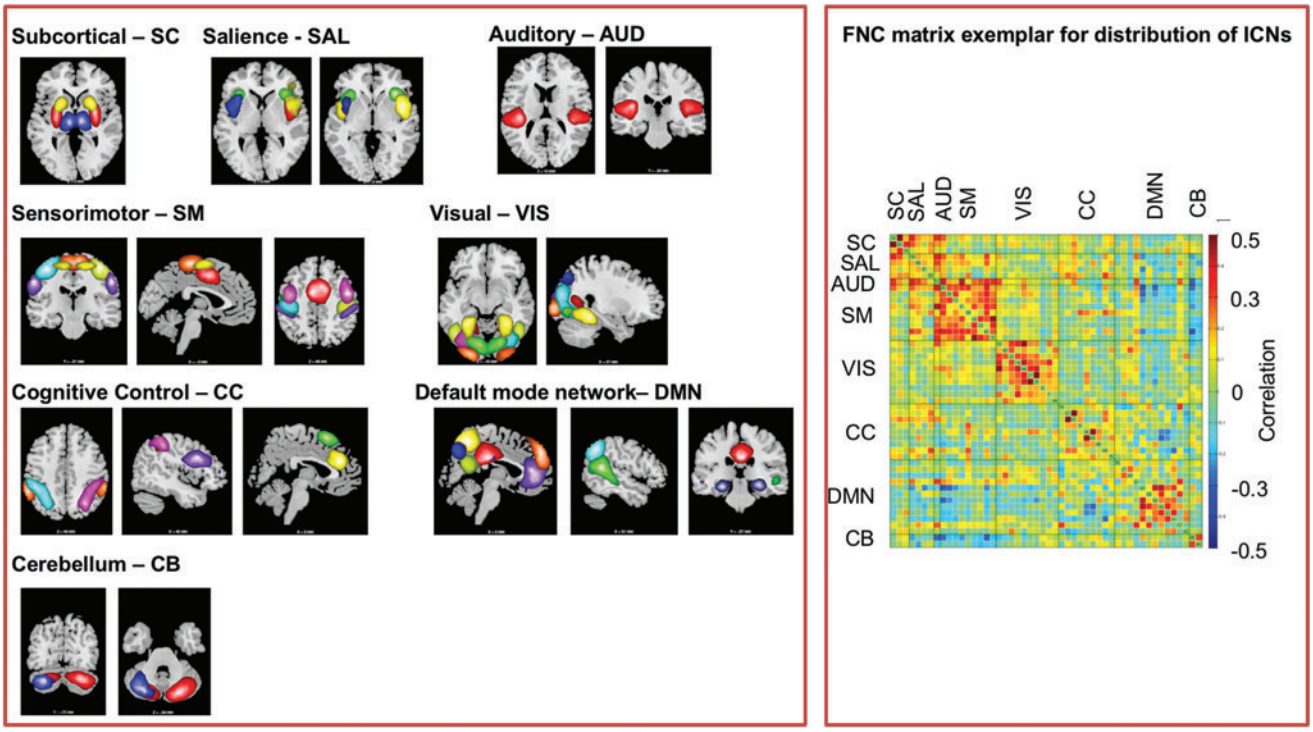

FIG. 2. Left: Functional domains and number of assigned ICNs, right: FNC matrix exemplar. ICN, intrinsic connectivity network. Color images are available online.

with white matter, ventricles, blood vessels, and nonbrain structures; and obeyed the expected power law, that is, showing exponentially higher power at the lowest frequencies and lowest power at the highest frequencies.

Inspection of the 100 independent components yielded 47 meaningful ICNs that were assigned to eight functional domains based on scientific literature (http://neurosynth.org) shown in Figure 2: SC, SAL, AUD, sensorimotor (SM), VIS, CC, DMN, and CB. Figure 2 shows all functional domains and Table 3 gives specific ICNs assigned to each domain.

Postprocessing of time courses. Postprocessing of time courses included linear, quadratic, and cubic detrending and regression of motion parameters (in x-, y-, and z-direction as well as pitch, roll, and yaw) as well as their derivatives and squares, in a single multiple regression framework (Power et al., 2014). Time courses were also despiked, defining spikes as time points with a root mean square of the framewise displacement >0.5 mm. These were identified based on the 3Ddespike algorithm as implemented in Analysis of Functional NeuroImages (Cox, 1996) and interpolated using a third order spline fit to ''clean'' neighboring data. Temporal filtering was applied with a bandpass fifth order Butterworth filter (passband 0.01–0.15 Hz). FNC was computed after postprocessing.

Dynamic functional network connectivity. We applied a sliding temporal window approach to rs-fMRI data to capture fluctuations of functional connectivity as proposed by Allen and colleagues (2012). A rectangular window (width 22 TRs)

Table 3. All Meaningful Intrinsic Connectivity Networks Assigned to Eight Functional Domains

Subcortical domain (SC)—three components	Bilateral putamen
	Bilateral thalamus
	Bilateral putamen
Salience domain (SAL)—four components	Bilateral insular cortices
	Left insular cortex
	Right insular cortex
	Bilateral anterior insulae
Auditory domain (AUD)—one component	Bilateral superior temporal gyri
Sensory-motor domain (SM)—nine components	Bilateral supplementary motor area (SMA)
	Bilateral superior parietal cortices
	Bilateral superior frontal gyri
	Bilateral postcentral gyri
	Bilateral motor cortices
	Left motor cortex
	Bilateral somatosensory cortices
	Bilateral supramarginal gyri
	Right postcentral gyrus
Visual domain (VIS)—nine components	Bilateral calcarine sulci
	Bilateral middle occipital gyri
	Bilateral fusiform gyri
	Bilateral lingual gyri
	Bilateral middle occipital gyri
	Bilateral middle occipital gyri
	Bilateral inferior occipital gyri
	Cuneus
	Bilateral inferior occipital gyri
Cognitive control domain (CC)—eight components	Left inferior frontal gyrus
	Bilateral middle frontal gyri
	Bilateral dorsal anterior cingulate cortices (dACC)
	Bilateral presupplementary motor area (preSMA)
	Bilateral posterior parietal cortices
	Left posterior parietal cortex
	Bilateral inferior parietal lobule
	Bilateral inferior frontal gyri
Default mode domain (DMN)—11 components	Medial posterior cingulate cortex
	Bilateral precuneus
	Bilateral precuneus
	Right temporoparietal junction
	Left angular gyrus
	Right angular gyrus
	Medial superior frontal gyrus
	Rostral anterior cingulate cortex
	Bilateral precunei
	Left temporoparietal junction
	Bilateral parahippocampal gyri
Cerebellar domain (CB)—two components	Bilateral cerebellum
	Left cerebellum

was convolved with a Gaussian of sigma three TRs to obtain tapering along the edges of the window, which is advantageous in signal processing terms. This tapered window slid in steps of one TR across concatenated time courses. For all windows, separate FNC matrices consisting of cross-correlations of ICN time courses were calculated. As shown in Figure 1, windows with highest variance in FNC, that is, local extrema in the global deviation from the subject's mean connectivity, are chosen from each subject (subject exemplars) for initial k-means clustering across all groups yielding cluster centroids. Based on the elbow criterion (ratio of within- to between-cluster distances), the optimal number of distinguishable whole-brain connectivity patterns (=states) was estimated to be 5. Cluster centroids were then used as starting points to cluster all windowed FNC matrices into five states: each windowed FNC matrix was assigned to the one cluster centroid it showed the highest correlation with.

Dynamic indices. Dynamic indices are measures summarizing the dynamic pattern across the resting-state scan numerically. The NTs reflects how often an individual changes discrete dynamic states. The fraction of time (FT) of a specific dynamic state is computed based on the total time spent in a given state divided by the total scan time. The average time (in windows) spent in a state before transitioning to another state is called MDT. Furthermore, we calculated the likelihood for transitioning from one state to another, which is summarized in a transition matrix (TM; size ''number of states'' by ''number of states'', i.e., 5×5).

For each dynamic index, we computed a one-way analysis of variance (ANOVA) to identify group effects. Critical p values for FT and MDT were $p<0.01$ (i.e., 0.05/5) applying Bonferroni correction to protect an alpha level of 0.05 when performing five tests. For the TM one-way ANOVA, we applied a Bonferroni-corrected p value of <0.002 (i.e., 0.05/25); multiple comparison correction was not necessary for NT since it is one measure per subject and just one test is performed.

Multistate relationship. First, we tested whether there are significant group differences in the overall connectivity pattern in each one of the five distinct states between groups. Therefore, we performed a multivariate ANOVA on all dimension-reduced states. Dimension reduction is a necessary step to avoid multicollinearity. Significant results in all states motivated further univariate analysis.

Since we were, in particular, interested in whether connectivity changes across states occur equally across the groups within each ICN×ICN pair, we performed a 3×5 ANOVA, including the factors group (factor levels: HC, CHR, and ESZ) and state (factor level: states 1, 2, 3, 4, and 5). We applied Bonferroni correction to correct for multiple comparisons. The critical p value for significance was $0.001/(3\times1081)$ at an alpha level of 0.05, that is, alpha level/number of cells in the FNC matrix that were tested for two main effects and the interaction of both. The interaction was further followed up by performing two separate one-way ANOVAs: one for the simple effects of state within each group and one for the simple effect of group within each state. Again, we applied conservative Bonferroni correction

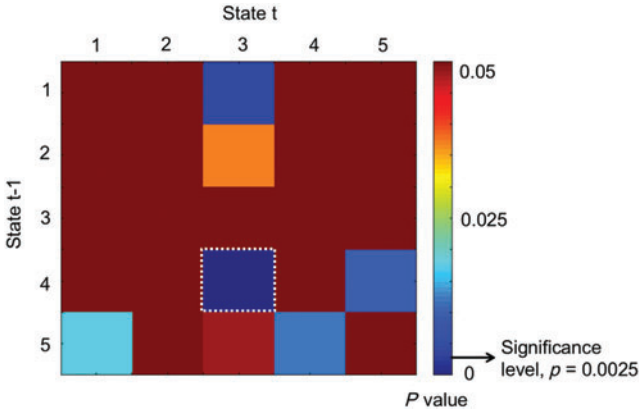

FIG. 3. Plotted p values for transition matrix analysis of variance; significant group effect in dotted square. Color images are available online.

considering all performed tests: the first one-way ANOVA included 10 tests, that is, state 1–state2, state 1–state 3, etc., the second one-way ANOVA encompassed three tests per state, that is, HC–CHR, HC–ESZ, and CHR–ESZ. Since 10 ICN pairs showed a significant interaction effect and ANOVAs were just performed on those, the critical p values were as follows: $0.05/(10\times10)$ for the first one-way ANOVA and $0.05/(10\times3)$ for the second one-way ANOVA. Significant results from this analysis were further evaluated by applying Tukey's HSD tests as implemented in the Matlab (7.12.0 [R2011a]; The MathWorks, Inc., Natick, MA) function multcompare to evaluate which states and groups, respectively, differed significantly.

Additional analysis on medication effects in CHR and ESZ groups can be found in the Supplementary Data.

Association between connectivity and symptom severity. To investigate possible associations between functional connectivity strength and symptom severity, we computed bivariate Pearson correlations for CHR and ESZ groups. Positive and negative symptom scores based on SOPS (McGlashan et al., 2001; Miller et al., 2003) for CHR individuals and PANSS (Kay et al., 1987) for ESZ individuals were correlated with the cell-wise connectivity in each state. Results were considered significant below a p value of 4.63×10^{-5}, that is, 0.05/1081 (alpha level/number of cells in the FNC matrix; Bonferroni correction). Clinical data that were used were collected within 2 weeks after the resting-

TABLE 4. SIGNIFICANT GROUP EFFECT FOR TRANSITION MATRIX ANALYSIS OF VARIANCE, *POST HOC* TUKEY'S HSD TEST RESULT

	Mean transition rate			p *value* post hoc *comparison*		
	HC	*CHR*	*ESZ*	*HC–CHR*	*HC–ESZ*	*CHR–ESZ*
State 4 to state 3	0.008	0	0.058	n.s.	0.0008	0.0002

n.s., non significant.

Table 5. Means and Standard Deviation for Mean Dwell Time, Fraction of Time, and Number of Transitions

State	*HC*	*CHR*	*ESZ*
Mean dwell time			
1	17.26 (25.5)	22.09 (33.5)	23.53 (37.8)
2	15.19 (32.4)	17.43 (32.9)	18.27 (37.1)
3	17.47 (23.7)	21.08 (29.6)	18.18 (24.2)
4	16.89 (27.6)	16.51 (33.7)	15.69 (23.4)
5	19.91 (25.7)	16.47 (24.5)	19.15 (29.5)
Fraction of time			
1	0.22 (0.26)	0.25 (0.31)	0.22 (0.29)
2	0.15 (0.27)	0.17 (0.27)	0.18 (0.3)
3	0.21 (0.26)	0.26 (0.29)	0.21 (0.25)
4	0.18 (0.27)	0.15 (0.29)	0.16 (0.22)
5	0.24 (0.27)	0.17 (0.25)	0.24 (0.3)
Number of transitions			
NT	4.4 (2.5)	3.8 (2.3)	4.2 (2.8)

state scan; data were available for 42 CHR and 56 ESZ individuals for these analyses.

Results

The five distinct dFNC states

Results regarding dFNC are based on correlation matrices representing intercomponent connectivity (ICN × ICN = 47 × 47 matrix), which can be further divided into functional domains. We identified five discrete dFNC states (Fig. 1) that vary with regard to their connectivity patterns. In HC and ESZ groups, state 5 was most common (24% and 23%, respectively, of all windows were assigned to this state), whereas state 3 was the most frequent state in CHR individuals (26% of all windows).

State 1. State 1 displays positive intradomain connectivity within each functional domain and negative connectivity between DMN and SC, SAL, AUD, SM, VIS, and CC domains as well as between CB and SAL, AUD, and SM domains. It also shows similarities with connectivity patterns typically found in static FNC analyses and we used it as a reference point to describe the other states.

State 2. State 2 shows less structured connectivity patterns across all functional domains compared with other states. Whole-brain connectivity is decreased. Maximum intradomain connectivity is found in SC, SAL, and SM domains, whereas interdomain connectivity is attenuated.

State 3. State 3 shows intra- and interdomain connectivity similar to state 1 with negative connectivity between the DMN and other functional domains and higher connectivity within each functional domain but overall to a lesser degree compared with state 1.

State 4. State 4 is characterized by the most distinct intra- and interdomain connectivity patterns. Positive intradomain connectivity within SM and VIS domains is more pronounced than in state 1. Anticorrelation between the DMN domain and other functional domains is weakened. Instead, SC areas show anticorrelation with sensorimotor areas and the CB shows strong anticorrelation with AUD, SM, and parts of the DMN domains.

State 5. Compared with state 1, state 5 shows decreased connectivity within the SM domain and increased positive connectivity within the VIS domain. Furthermore, only parts of the DMN domain show anticorrelation to SC, SAL, AUD, SM, VIS, and CC domains.

Dynamic indices

The likelihood of transitions between states showed significant group differences. The ESZ group exhibited increased likelihood of transitioning from state 4, a hyperconnected state, to state 3, a more ''loosely connected'' state, compared with HC ($p = 0.0008$) and CHR ($p = 0.0002$), see Figure 3 and Table 4.

ANOVAs for FT, MDT, and did not yield significant group differences, Table 5.

Multistate relationship

Multivariate analysis of variance. We tested each state's overall connectivity pattern for group differences. Significant results are presented in Table 6 and motivated further univariate tests.

Group × state ANOVA. Ten ICN pairs showed significant group by state interactions and were further followed up, details are presented in Table 7. These ICN pairs were assigned to the SC, DMN, AUD, SM, CC, and CB domains.

One-way ANOVA for state effects. Details are provided in Tables 8 and 9. In the HC group, 9 out of the 10 ICN pairs with a significant interaction effect showed significant connectivity differences across states. In the CHR group, 6 out of the 10 ICN pairs exhibited significant connectivity differences between states and 3 out of the 10 ICN pairs showed significant state effects in the ESZ group.

One out of the 10 ICN pairs that exhibited a significant group by state interaction effect showed significant connectivity changes in ESZ patients but in no other group (posterior parietal cortices [CC]–superior frontal gyrus medial [DMN]).

Table 6. Multivariate Analysis of Variance Results on Whole-Brain Connectivity Pattern in Each State *p* Values and *F*-Statistics for 3 × 5 Analysis of Variance

	State				
	1	*2*	*3*	*4*	*5*
p Value 1	2.79e-14	0.0122	4.06×10^{-4}	5.77×10^{-18}	1.53×10^{-14}
p Value 2	0.002	0.0451	0.085	0.0023	0.0011

Table 7. Intrinsic Connectivity Network Pairs Showing Significant Interaction Group by State in 3×5 Analysis of Variance

ICN 1	*ICN 2*	p *Value**	F-*statistics*
Superior temporal gyrus R+L (AUD)	Postcentral gyrus R+L (SM)	4.52×10^{-8}	6.5
Superior temporal gyrus R+L (AUD)	Superior frontal gyrus medial (DMN)	2.53×10^{-7}	5.96
Superior temporal gyrus R+L (AUD)	TPJ L (DMN)	1.15×10^{-7}	6.21
Thalamus R+L (SC)	Superior temporal gyrus R+L (AUD)	7.24×10^{-9}	7.06
SMA (SM)	Postcentral gyrus R (SM)	2.51×10^{-9}	7.39
Postcentral gyrus R+L (SM)	Postcentral gyrus R (SM)	7.01×10^{-8}	6.36
Postcentral gyrus R+L (SM)	TPJ L (DMN)	2.07×10^{-10}	8.16
Supramarginal gyrus R+L (SM)	TPJ L (DMN)	5.26×10^{-8}	6.45
Posterior parietal cortex R+L (CC)	Superior frontal gyrus medial (DMN)	2.74×10^{-7}	5.94
TPJ L (DMN)	Cerebellum R+L (CB)	5.19×10^{-9}	7.17

*Critical p value: 3.08×10^{-7}.
ICN, intrinsic connectivity network; SC, subcortical domain; AUD, auditory domain; DMN, default network domain; SM, sensorimotor domain; CC, cognitive control domain; CB, cerebellar domain; TPJ, temporoparietal junction; SMA, supplementary motor area.

In 7 out of the 10 ICN pairs with significant interaction effects where HC individuals exhibited significant changes of connectivity across states, connectivity changes were completely absent in ESZ patients: superior temporal gyri (STG; AUD)–postcentral gyri (SM), STG (AUD)–medial superior frontal gyrus (DMN), STG (AUD)–left temporoparietal junction (TPJ; DMN), postcentral gyri (SM)–right postcentral gyrus (SM), thalamus (SC)–STG (AUD), supramarginal gyri (SM)–left TPJ (DMN), and left TPJ (DMN)–CB. ICN pairs with significant state effects were further investigated by means of *post hoc* Tukey's HSD tests to determine which states differed significantly from each other with respect to their connectivity, for details see Figure 4(1–10).

One-way ANOVA for group effects. Details are provided in Tables 10 and 11 and Figure 4(1–10). States 1 and 4 revealed the most differences in connectivity between groups with eight and nine ICN pairs showing significant group effects. *Post hoc* Tukey's test revealed that in state 1, CHR and ESZ individuals exhibited significant dysconnectivity compared with HC individuals in all significant ICN pairs. In state 4, ESZ patients showed significant dysconnectivity compared with HC and CHR individuals in all but one ICN pair, that is, STG (AUD)–medial superior frontal gyrus (DMN) as indicated by *post hoc* Tukey's tests. States 2, 3, and 5 revealed group effects in only 1 out of the 10 ICN pairs. In state 2, STG (AUD)–medial superior frontal gyrus (DMN) exhibited significant differences between HC and CHR groups, and between CHR and ESZ groups. Posterior parietal cortices (CC)–medial superior frontal gyrus (DMN) revealed significant differences between the ESZ group and both the HC and CHR groups in state 3. In state 5, CHR and ESZ groups showed significantly altered connectivity compared with HC individuals between thalamus (SC)–STG (AUD).

Table 8. Results from the One-Way Analysis of Variance with the Factor "State," That Is, If the Intrinsic Connectivity Network Pair Shows Significant Changes in Connectivity Across States

		p *Value**			F-*statistics*		
ICN 1	*ICN 2*	*HC*	*CHR*	*ESZ*	*HC*	*CHR*	*ESZ*
Superior temporal gyrus R+L (AUD)	Postcentral gyrus R+L (SM)	8.14×10^{-8}	n.s.	n.s.	10.6	—	—
Superior temporal gyrus R+L (AUD)	Superior frontal gyrus medial (DMN)	4.48×10^{-20}	8.52×10^{-5}	n.s.	30.94	6.44	—
Superior temporal gyrus R+L (AUD)	TPJ L (DMN)	4.26×10^{-9}	2.71×10^{-5}	n.s.	12.5	7.17	—
Thalamus R+L (SC)	Superior temporal gyrus R+L (AUD)	3.14×10^{-18}	2.4×10^{-4}	n.s.	27.53	5.79	—
SMA (SM)	Postcentral gyrus R (SM)	1.07×10^{-9}	n.s.	1.41×10^{-4}	13.4	—	6.06
Postcentral gyrus R+L (SM)	Postcentral gyrus R (SM)	2.3×10^{-13}	n.s.	n.s.	19.16	—	—
Postcentral gyrus R+L (SM)	TPJ L (DMN)	1.81×10^{-11}	7.46×10^{-6}	5.64×10^{-5}	16.12	8.01	6.63
Supramarginal gyrus R+L (SM)	TPJ L (DMN)	2.87×10^{-7}	1.83×10^{-6}	n.s.	9.81	8.93	—
Posterior parietal cortex R+L (CC)	Superior frontal gyrus medial (DMN)	n.s.	n.s.	5.52×10^{-12}	—	—	17.47
TPJ L (DMN)	Cerebellum R+L (CB)	1.38×10^{-12}	2.16×10^{-7}	n.s.	17.9	10.35	—

*Critical p value: 5.00×10^{-4}.

Table 9. Summary of Significant Intrinsic Connectivity Network Pairs for Healthy Controls, Clinical High Risk, and Early Illness Schizophrenia Groups

ICN 1	*ICN 2*
HC	
Superior temporal gyrus R + L (AUD)	Postcentral gyrus R + L (SM)
Superior temporal gyrus R + L (AUD)	Superior frontal gyrus medial (DMN)
Superior temporal gyrus R + L (AUD)	TPJ L (DMN)
Thalamus R + L (SC)	Superior temporal gyrus R + L (AUD)
SMA (SM)	Postcentral gyrus R (SM)
Postcentral gyrus R + L (SM)	Postcentral gyrus R (SM)
Postcentral gyrus R + L (SM)	TPJ L (DMN)
Supramarginal gyrus R + L (SM)	TPJ L (DMN)
TPJ L (DMN)	Cerebellum R + L (CB)
CHR	
Superior temporal gyrus R + L (AUD)	Superior frontal gyrus medial (DMN)
Superior temporal gyrus R + L (AUD)	TPJ L (DMN)
Thalamus R + L (SC)	Superior temporal gyrus R + L (AUD)
Postcentral gyrus R + L (SM)	TPJ L (DMN)
Supramarginal gyrus R + L (SM)	TPJ L (DMN)
TPJ L (DMN)	Cerebellum R + L (CB)
ESZ	
SMA (SM)	Postcentral gyrus R (SM)
Postcentral gyrus R + L (SM)	TPJ L (DMN)
Posterior parietal cortex R + L (CC)	Superior frontal gyrus medial (DMN)

Association between connectivity and symptom severity

No significant associations between state-specific FNC and clinical ratings were obtained applying a Bonferroni-corrected threshold.

Discussion

In this study, we extended the existing framework of dysconnectivity in schizophrenia and the psychosis risk syndrome by applying a sliding temporal window approach and k-means clustering to yield distinct connectivity states and dynamic indices characterizing dynamic behavior as suggested by Allen and associates (2012). In our study, ESZ patients exhibited an increased likelihood of transitioning from a hyperconnected state to a ''loosely connected'' state compared with HC and CHR individuals. In ICN pairs with a significant group by state interaction effect, HC individuals showed significant changes of connectivity between states that were absent or altered in ESZ and CHR individuals. Connectivity differences between groups have been found primarily in two out of the five states. In summary, it appears that the interaction effect was mostly driven by (1) dynamic connectivity changes in HC that were abnormal in CHR and ESZ individuals and (2) the fact that dysconnectivity between groups was only present in some states. These findings underscore the likelihood that abnormalities not only in static FNC but also in dFNC are present in CHR and ESZ individuals.

Dynamic indices

The ESZ group showed significantly higher likelihood than HC and CHR groups to transition from state 4, a hyperconnected state, to state 3, a more loosely connected state, that is, whole-brain connectivity within and between domains is either heightened (state 4) or decreased (state 3). As shown by Damaraju and colleagues (2014), patients with chronic schizophrenia tend to spend more time in loosely connected states as well. Damaraju and associates' (2014) report is complemented by the current finding that ESZ patients are more likely to transition to the loosely connected state 3 from state 4 even though ESZ patients do not spend more time in this state as indicated by a non-significant difference in MDT. However, state 4 in our study is also characterized by cortical–SC antagonism. As Damaraju and colleagues (2014) described, (1) patients with chronic schizophrenia had fewer transitions to states showing this feature and (2) dysconnectivity captured in these states was more pronounced. Furthermore, these authors argue that cortical–SC antagonism co-occurs with thalamic hyperconnectivity. Thalamic hyperconnectivity is a consistent finding in static FNC analyses in patients with schizophrenia (Anticevic et al., 2014; Damaraju et al., 2014; Woodward et al., 2012) as well as in CHR individuals (Anticevic et al., 2015; Ferri et al., 2017) that predicts symptoms in patients with schizophrenia (Anticevic et al., 2014) and transition to psychosis in CHR individuals (Anticevic et al., 2015). Given these results, it appears that patients with schizophrenia exhibit (1) fewer occurrences (Damaraju et al., 2014) of brain states with a hyperconnected whole-brain connectivity pattern accompanied by cortical–SC antagonism that has been related to increased thalamic dysconnectivity and (2) ESZ patients lingering in such a state exhibit increased likelihood of transitioning to a loosely connected state (shown by this study). The differences observed between Damaraju and colleagues' (2014) study and our study might be due to the difference in illness duration of patients studied (chronic vs. within 5 years after illness onset). Overall, these findings were only detectable by applying a dynamic approach. However, the functional meaning of transitioning between brain states has to be further investigated in future studies.

Since ESZ and CHR individuals did not exhibit significant abnormalities in any of the other indices capturing dynamic behavior of FNC, it appears that the dynamic behavior as captured with these metrics is not a major domain of pathophysiology in schizophrenia or the psychosis risk syndrome.

Multistate relationship

Unlike previous studies on dFNC that applied state-wise comparisons of groups (Damaraju et al., 2014; Rashid et al., 2014), we rather investigated the interaction of group and state on each of the ICN connectivity pairs to test for differences in the dynamic behavior of connectivity. Results were further analyzed to disentangle the interaction

effect by separate one-way ANOVAs with state and group as factors, respectively.

State effects. Connectivity between posterior parietal cortices (CC) and medial superior frontal gyrus (DMN) exhibited significant connectivity changes in ESZ patients but in no other group. In general, dysconnectivity between the CC domain and the DMN has been reported numerous times in schizophrenia in comparison with HC individuals and has been related to cognitive deficits in patients with schizophrenia (Hasenkamp et al., 2011; Manoliu et al., 2014; Whitfield-Gabrieli and Ford, 2012; Whitfield-Gabrieli et al., 2009). However, findings from this study lead to the conclusion that in addition to state-dependent dysconnectivity, the dynamic behavior of connectivity between these brain areas is altered in ESZ patients. Furthermore, these alterations are not observed in CHR individuals. Assuming an association between functional dysconnectivity and cognitive deficits, this finding is in line with a recent review on synaptic plasticity (Forsyth and Lewis, 2017) that hypothesized that impairments in the cognitive domain might appear late during the prodromal phase of schizophrenia.

In 7 out of the 10 ICN pairs with significant interaction effects where HC individuals exhibited significant changes of connectivity across states, connectivity changes were completely absent in ESZ patients. The STG and left TPJ seem to be ''hotspots'' of aberrant dynamic behavior of connectivity as they appear in six out of the seven ICN pairs. Connectivity between them as well as connectivity with parts of the SM domain (postcentral and supramarginal gyri) and the thalamus appears affected in ESZ patients. Both regions, STG and left TPJ, have been found to be associated with dysconnectivity in schizophrenia patients experiencing AUD verbal hallucinations (Alderson-Day et al., 2015; Jardri et al., 2011; Thoma et al., 2016; Vercammen et al., 2010). In this study, there were no significant associations between positive symptom scores and connectivity in ESZ and CHR groups, rendering it likely that these networks play a more general disease-relevant role.

CHR individuals exhibited either fewer significant changes or changes between different states than HC individuals in most ICN pairs with a significant interaction effect. Furthermore, dynamic changes of connectivity were absent between the STG and postcentral gyri (SM), SMA

1) Superior Temporal Gyrus R+L (AUD) – Postcentral Gyrus R+L (SM)

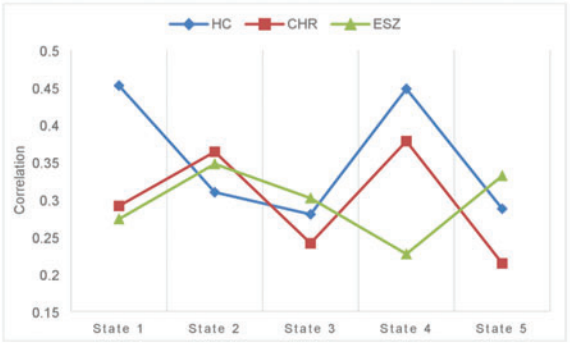

i) P-values of state effect in each group (Tukey's HSD tests)

State Comparison	Group		
	HC	CHR	ESZ
State 1 – State 2	0.0042	n.s.	n.s.
State 1 – State 3	2.56×10^{-05}	n.s.	n.s.
State 1 – State 4	n.s.	n.s.	n.s.
State 1 – State 5	4.44×10^{-05}	n.s.	n.s.
State 2 – State 3	n.s.	n.s.	n.s.
State 2 – State 4	0.0095	n.s.	n.s.
State 2 – State 5	n.s.	n.s.	n.s.
State 3 – State 4	0.0001	n.s.	n.s.
State 3 – State 5	n.s.	n.s.	n.s.
State 4 – State 5	0.0002	n.s.	n.s.

ii) P-values of group effect in each state (Tukey's HSD tests)

Group comparison	State				
	1	2	3	4	5
HC – CHR	8.65×10^{-05}	n.s.	n.s.	n.s.	n.s.
HC – ESZ	1.72×10^{-05}	n.s.	n.s.	1.52×10^{-06}	n.s.
CHR – ESZ	n.s.	n.s.	n.s.	0.0093	n.s.

2) Superior Temporal Gyrus R+L (AUD) – Superior Frontal Gyrus medial (DMN)

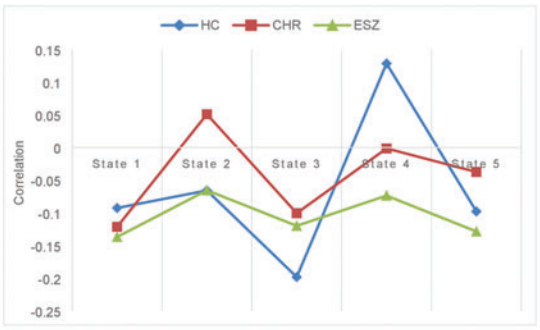

i) P-values of state effect in each group (Tukey's HSD tests)

State comparison	Group		
	HC	CHR	ESZ
State 1 – State 2	n.s.	9.61×10^{-05}	n.s.
State 1 – State 3	0.002	n.s.	n.s.
State 1 – State 4	9.92×10^{-09}	0.0404	n.s.
State 1 – State 5	n.s.	n.s.	n.s.
State 2 – State 3	0.0002	0.001	n.s.
State 2 – State 4	4.45×10^{-08}	n.s.	n.s.
State 2 – State 5	n.s.	n.s.	n.s.
State 3 – State 4	9.92×10^{-09}	n.s.	n.s.
State 3 – State 5	0.0023	n.s.	n.s.
State 4 – State 5	9.92×10^{-09}	n.s.	n.s.

ii) P-values of group effect in each state (Tukey's HSD tests)

Group comparison	State				
	1	2	3	4	5
HC – CHR	n.s.	0.0033	n.s.	0.0086	n.s.
HC – ESZ	n.s.	n.s.	n.s.	2.62×10^{-07}	n.s.
CHR – ESZ	n.s.	0.0056	n.s.	n.s.	n.s.

FIG. 4. Plots for each ICN pair showing a significant interaction effect group by state and results from *post hoc* Tukey's HSD tests for state and group effects. **(1)** Superior Temporal Gyrus-Postcentral Gyrus; **(2)** Superior Temporal Gyrus-Superior Frontal Gyrus medial; **(3)** Superior Temporal Gyrus-TPJ; **(4)** Thalamus-Superior Temporal Gyrus; **(5)** SMA-Postcentral Gyrus; **(6)** Postcentral Gyrus-Postcentral Gyrus; **(7)** Postcentral Gyrus-TPJ; **(8)** Supramarginal Gyrus-TPJ; **(9)** Posterior Parietal Cortex-Superior Frontal Gyrus; **(10)** TPJ-Cerebellum. **(i)** *p*-values of state effect in each group; **(ii)** *p*-values of group effect in each state. AUD, auditory domain; SM, sensorimotor domain; DMN, default mode network; CC, cognitive control domain; CB, cerebellar domain; SC, subcortical domain; TPJ, temporoparietal junction; CHR, clinical high risk; ESZ, early illness schizophrenia; HC, healthy control. Color images are available online.

3) Superior Temporal Gyrus R+L (AUD) – TPJ L (DMN)

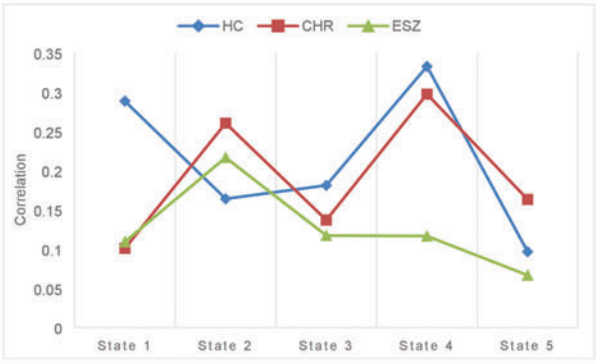

i) P-values of state effect in each group (Tukey's HSD tests)

State comparison	Group		
	HC	CHR	ESZ
State 1 – State 2	0.0229	0.001	n.s.
State 1 – State 3	0.0333	n.s.	n.s.
State 1 – State 4	n.s.	0.0001	n.s.
State 1 – State 5	1.65×10^{-06}	n.s.	n.s.
State 2 – State 3	n.s.	0.0222	n.s.
State 2 – State 4	0.0009	n.s.	n.s.
State 2 – State 5	n.s.	n.s.	n.s.
State 3 – State 4	0.001	0.0034	n.s.
State 3 – State 5	n.s.	n.s.	n.s.
State 4 – State 5	1.84×10^{-08}	0.0347	n.s.

ii) P-values of group effect in each state (Tukey's HSD tests)

Group comparison	State				
	1	2	3	4	5
HC – CHR	6.13×10^{-06}	n.s.	n.s.	n.s.	n.s.
HC – ESZ	2.06×10^{-05}	n.s.	n.s.	1.36×10^{-07}	n.s.
CHR – ESZ	n.s.	n.s.	n.s.	0.0003	n.s.

4) Thalamus R+L (SC) – Superior Temporal Gyrus R+L (AUD)

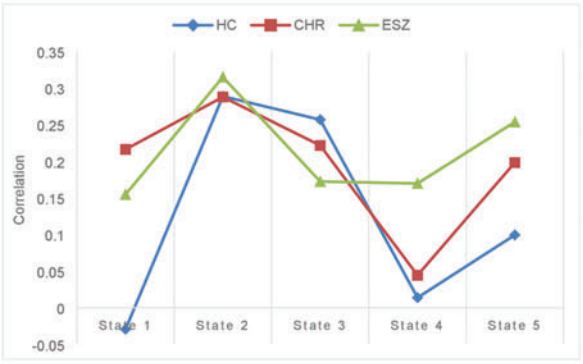

i) P-values of state effect in each group (Tukey's HSD tests)

State comparison	Group		
	HC	CHR	ESZ
State 1 – State 2	9.92×10^{-09}	n.s.	n.s.
State 1 – State 3	9.92×10^{-09}	n.s.	n.s.
State 1 – State 4	n.s.	0.003	n.s.
State 1 – State 5	0.0023	n.s.	n.s.
State 2 – State 3	n.s.	n.s.	n.s.
State 2 – State 4	1.02×10^{-08}	2.90×10^{-05}	n.s.
State 2 – State 5	8.84×10^{-06}	n.s.	n.s.
State 3 – State 4	1.08×10^{-08}	0.002	n.s.
State 3 – State 5	4.77×10^{-05}	n.s.	n.s.
State 4 – State 5	n.s.	0.017	n.s.

ii) P-values of group effect in each state (Tukey's HSD tests)

Group comparison	State				
	1	2	3	4	5
HC – CHR	1.19×10^{-09}	n.s.	n.s.	n.s.	0.0168
HC – ESZ	1.72×10^{-06}	n.s.	n.s.	0.0011	2.79×10^{-05}
CHR – ESZ	n.s.	n.s.	n.s.	0.0456	n.s.

5) SMA (SM) – Postcentral Gyrus R (SM)

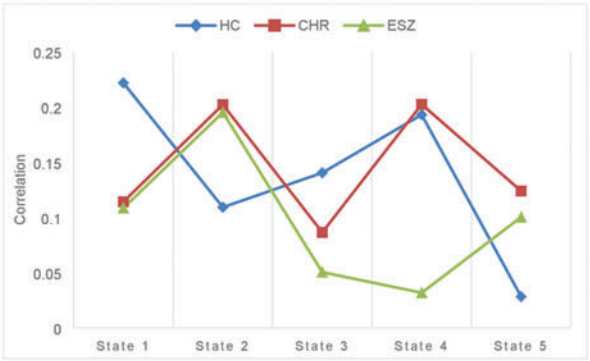

i) P-values of state effect in each group (Tukey's HSD tests)

State comparison	Group		
	HC	CHR	ESZ
State 1 – State 2	0.005	n.s.	n.s.
State 1 – State 3	0.0459	n.s.	n.s.
State 1 – State 4	n.s.	n.s.	n.s.
State 1 – State 5	1.01×10^{-08}	n.s.	n.s.
State 2 – State 3	n.s.	n.s.	0.0007
State 2 – State 4	n.s.	n.s.	6.29×10^{-05}
State 2 – State 5	n.s.	n.s.	n.s.
State 3 – State 4	n.s.	n.s.	n.s.
State 3 – State 5	0.0008	n.s.	n.s.
State 4 – State 5	6.04×10^{-07}	n.s.	n.s.

ii) P-values of group effect in each state (Tukey's HSD tests)

Group comparison	State				
	1	2	3	4	5
HC – CHR	0.0017	n.s.	n.s.	n.s.	n.s.
HC – ESZ	0.0011	n.s.	n.s.	1.19×10^{-05}	n.s.
CHR – ESZ	n.s.	n.s.	n.s.	0.0002	n.s.

6) Postcentral Gyrus R+L (SM) – Postcentral Gyrus R (SM)

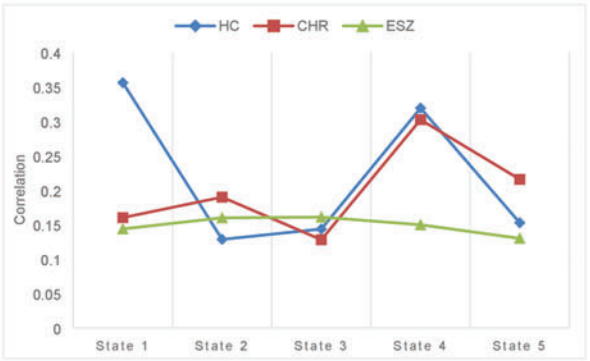

i) P-values of state effect in each group (Tukey's HSD tests)

State comparison	Group		
	HC	CHR	ESZ
State 1 – State 2	1.88×10^{-08}	n.s.	n.s.
State 1 – State 3	1.19×10^{-08}	n.s.	n.s.
State 1 – State 4	n.s.	n.s.	n.s.
State 1 – State 5	1.53×10^{-08}	n.s.	n.s.
State 2 – State 3	n.s.	n.s.	n.s.
State 2 – State 4	7.97×10^{-06}	n.s.	n.s.
State 2 – State 5	n.s.	n.s.	n.s.
State 3 – State 4	5.55×10^{-06}	n.s.	n.s.
State 3 – State 5	n.s.	n.s.	n.s.
State 4 – State 5	1.34×10^{-05}	n.s.	n.s.

ii) P-values of group effect in each state (Tukey's HSD tests)

Group comparison	State				
	1	2	3	4	5
HC – CHR	5.89×10^{-07}	n.s.	n.s.	n.s.	n.s.
HC – ESZ	1.06×10^{-07}	n.s.	n.s.	0.0001	n.s.
CHR – ESZ	n.s.	n.s.	n.s.	0.006	n.s.

FIG. 4. (Continued).

7) Postcentral Gyrus R+L (SM) – TPJ L (DMN)

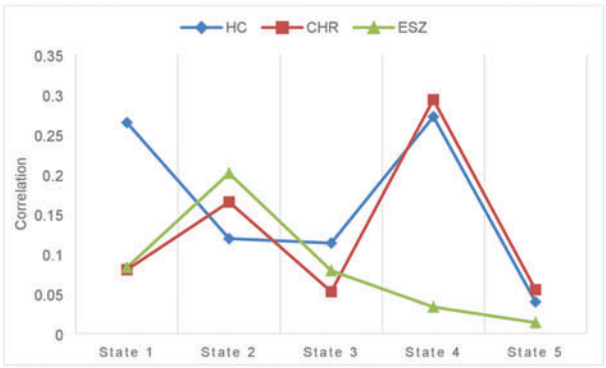

i) P-values of state effect in each group (Tukey's HSD tests)

State comparison	Group		
	HC	CHR	ESZ
State 1 – State 2	0.002	n.s.	0.022
State 1 – State 3	0.0002	n.s.	n.s.
State 1 – State 4	n.s.	0.0001	n.s.
State 1 – State 5	1.08×10^{-08}	n.s.	n.s.
State 2 – State 3	n.s.	n.s.	0.016
State 2 – State 4	0.0017	n.s.	0.0002
State 2 – State 5	n.s.	n.s.	1.58×10^{-05}
State 3 – State 4	0.0002	7.48×10^{-06}	n.s.
State 3 – State 5	n.s.	n.s.	n.s.
State 4 – State 5	1.17×10^{-08}	2.58×10^{-05}	n.s.

ii) P-values of group effect in each state (Tukey's HSD tests)

Group comparison	State				
	1	2	3	4	5
HC – CHR	5.25×10^{-06}	n.s.	n.s.	n.s.	n.s.
HC – ESZ	9.83×10^{-06}	n.s.	n.s.	4.64×10^{-09}	n.s.
CHR – ESZ	n.s.	n.s.	n.s.	1.12×10^{-07}	n.s.

8) Supramarginal Gyrus R+L (SM) – TPJ L (DMN)

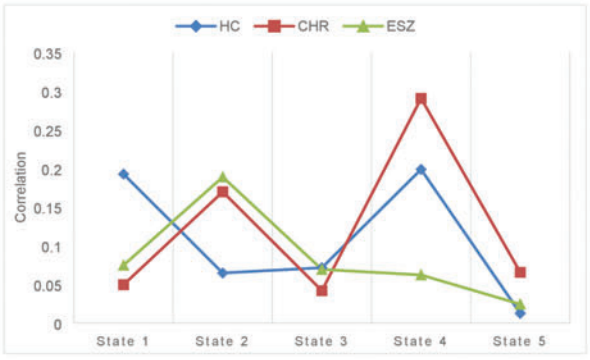

i) P-values of state effect in each group (Tukey's HSD tests)

State comparison	Group		
	HC	CHR	ESZ
State 1 – State 2	0.0147	n.s.	n.s.
State 1 – State 3	0.0087	n.s.	n.s.
State 1 – State 4	n.s.	7.12×10^{-06}	n.s.
State 1 – State 5	5.59×10^{-06}	n.s.	n.s.
State 2 – State 3	n.s.	0.0318	n.s.
State 2 – State 4	0.0137	n.s.	n.s.
State 2 – State 5	n.s.	n.s.	n.s.
State 3 – State 4	0.009	3.11×10^{-06}	n.s.
State 3 – State 5	n.s.	n.s.	n.s.
State 4 – State 5	8.53×10^{-06}	8.75×10^{-05}	n.s.

ii) P-values of group effect in each state (Tukey's HSD tests)

Group comparison	State				
	1	2	3	4	5
HC – CHR	0.0004	n.s.	n.s.	n.s.	n.s.
HC – ESZ	0.0046	n.s.	n.s.	0.0012	n.s.
CHR – ESZ	n.s.	n.s.	n.s.	8.50×10^{-06}	n.s.

9) Posterior Parietal Cortex R+L (CC) – Superior Frontal Gyrus medial (DMN)

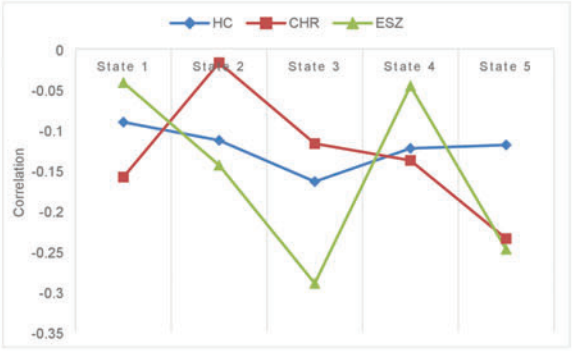

i) P-values of state effect in each group (Tukey's HSD tests)

State comparison	Group		
	HC	CHR	ESZ
State 1 – State 2	n.s.	n.s.	n.s.
State 1 – State 3	n.s.	n.s.	1.12×10^{-08}
State 1 – State 4	n.s.	n.s.	n.s.
State 1 – State 5	n.s.	n.s.	7.96×10^{-07}
State 2 – State 3	n.s.	n.s.	0.0056
State 2 – State 4	n.s.	n.s.	n.s.
State 2 – State 5	n.s.	n.s.	n.s.
State 3 – State 4	n.s.	n.s.	1.19×10^{-08}
State 3 – State 5	n.s.	n.s.	n.s.
State 4 – State 5	n.s.	n.s.	1.21×10^{-06}

ii) P-values of group effect in each state (Tukey's HSD tests)

Group comparison	State				
	1	2	3	4	5
HC – CHR	n.s.	n.s.	n.s.	n.s.	n.s.
HC – ESZ	n.s.	n.s.	0.0052	n.s.	n.s.
CHR – ESZ	n.s.	n.s.	0.0002	n.s.	n.s.

10) TPJ L (DMN) – Cerebellum R+L (CB)

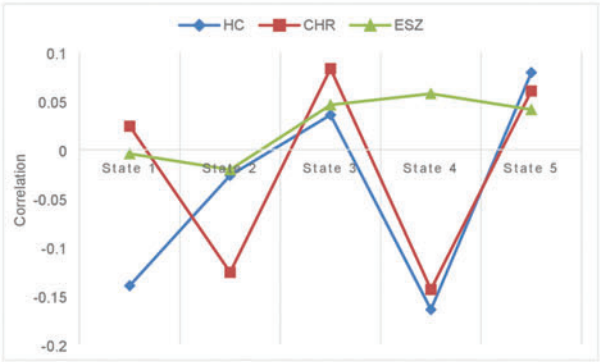

i) P-values of state effect in each group (Tukey's HSD tests)

State comparison	Group		
	HC	CHR	ESZ
State 1 – State 2	0.03	0.005	n.s.
State 1 – State 3	5.65×10^{-06}	n.s.	n.s.
State 1 – State 4	n.s.	0.0039	n.s.
State 1 – State 5	1.18×10^{-08}	n.s.	n.s.
State 2 – State 3	n.s.	1.39×10^{-05}	n.s.
State 2 – State 4	0.006	n.s.	n.s.
State 2 – State 5	0.0413	0.0004	n.s.
State 3 – State 4	5.56×10^{-07}	1.86×10^{-05}	n.s.
State 3 – State 5	n.s.	n.s.	n.s.
State 4 – State 5	1.01×10^{-08}	0.0004	n.s.

ii) P-values of group effect in each state (Tukey's HSD tests)

Group comparison	State				
	1	2	3	4	5
HC – CHR	1.60×10^{-05}	n.s.	n.s.	n.s.	n.s.
HC – ESZ	0.0005	n.s.	n.s.	9.08×10^{-08}	n.s.
CHR – ESZ	n.s.	n.s.	n.s.	6.28×10^{-05}	n.s.

FIG. 4. (Continued).

TABLE 10. RESULTS FROM ONE-WAY ANALYSIS OF VARIANCE WITH THE FACTOR "GROUP," THAT IS, IF THE INTRINSIC CONNECTIVITY NETWORK PAIR SHOWS SIGNIFICANT DIFFERENCES IN CONNECTIVITY BETWEEN GROUPS IN THAT SPECIFIC STATE

		p *Value**					F-*statistics*				
		State					*State*				
ICN 1	*ICN 2*	*1*	*2*	*3*	*4*	*5*	*1*	*2*	*3*	*4*	*5*
Superior temporal gyrus R + L (AUD)	Postcentral gyrus R + L (SM)	2.95×10^{-6}	n.s.	n.s.	2.27×10^{-6}	n.s.	14.27	—	—	15.12	—
Superior temporal gyrus R + L (AUD)	Superior frontal gyrus medial (DMN)	n.s.	0.0015	n.s.	4.69×10^{-7}	n.s.	—	7.06	—	17.28	—
Superior temporal gyrus R + L (AUD)	TPJ L (DMN)	6.51×10^{-7}	n.s.	n.s.	9.09×10^{-8}	n.s.	16.18	—	—	19.61	—
Thalamus R + L (SC)	Superior temporal gyrus R + L (AUD)	1.09×10^{-10}	n.s.	n.s.	0.001	3.38×10^{-5}	28.24	—	—	7.36	11.29
SMA (SM)	Postcentral gyrus R (SM)	2.66×10^{-4}	n.s.	n.s.	2.21×10^{-6}	n.s.	8.86	—	—	15.15	—
Postcentral gyrus R + L (SM)	Postcentral gyrus R (SM)	5.77×10^{-9}	n.s.	n.s.	8.08×10^{-5}	n.s.	22.51	—	—	10.51	—
Postcentral gyrus R + L (SM)	TPJ L (DMN)	3.8×10^{-7}	n.s.	n.s.	1.48×10^{-10}	n.s.	16.88	—	—	29.59	—
Supramarginal gyrus R + L (SM)	TPJ L (DMN)	2.07×10^{-4}	n.s.	n.s.	4.65×10^{-6}	n.s.	9.15	—	—	14.16	—
Posterior parietal cortex R + L (CC)	Superior frontal gyrus medial (DMN)	n.s.	n.s.	1.63×10^{-4}	n.s.	n.s.	—	—	9.41	—	—
TPJ L (DMN)	Cerebellum R + L (CB)	6.95×10^{-6}	n.s.	n.s.	3.51×10^{-8}	n.s.	13.2	—	—	21	—

*Critical p value: 0.0017.

and right postcentral gyrus (both SM), and within postcentral gyri (SM) in CHR individuals. This accumulation of dysconnectivity in the SM domain in CHR individuals might be a link to often observed motor impairments in CHR individuals (Van Harten et al., 2017) that also have been shown to predict conversion to psychosis (Callaway et al., 2014). Clearly, future studies are needed to specifically test this possibility.

Although merely descriptive, connectivity changes across states are present in HC individuals, are less frequent in CHR individuals, and are mostly absent in ESZ patients in the 10 ICN pairs exhibiting a significant group by state interaction, possibly reflecting a linear progression of dysconnectivity from an at-risk state to full-blown psychosis.

Group effects. Connectivity differences between groups have been captured by two states primarily: state 1 characterized by a whole-brain connectivity pattern with anticorrelation between the DMN and other functional domains, and state 4 that exhibited whole-brain hyperconnectivity concomitant with cortical–SC antagonism. Given the significant interaction effect, dysconnectivity between groups depends on the state that is being analyzed. Whereas state 1 captured significant differences in CHR and ESZ individuals compared with HC, state 4 revealed significant differences between the ESZ group compared with both HC and CHR individuals. In general, dysconnectivity in ESZ and CHR individuals was only prevalent in some states. This more precise depiction of dysconnectivity in schizophrenia and the psychosis risk syndrome could not have been achieved with a static FNC approach, wherein connectivity is summarized across the entire scan time. In such a static scenario, dysconnectivity, in particular in CHR individuals who showed a changing pattern of dysconnectivity depending on the state that is being analyzed, would have been over- or underestimated depending on which effect would have had more power, that is, the portion of the time course where CHR individuals do not show connectivity differences or the portion that does reveal such differences.

However, it is noteworthy that state 1, one of the two states showing dysconnectivity patterns between HC, CHR, and ESZ individuals, was most similar to static FNC.

Conclusion

We showed that dynamic behavior of connectivity with regard to FNC and dynamic indices appeared to be altered in ESZ patients and is mostly intact in CHR individuals. Considering a linear disease progression model with symptom aggravation from an at-risk mental state to full-blown psychosis (Cannon, 2015), current results can be interpreted as consistent with this model: CHR individuals show less severe abnormalities of FNC than ESZ patients.

Furthermore, dysconnectivity observed in schizophrenia patients exhibits a stable pattern across states, whereas dysconnectivity in CHR individuals depends on the dFNC state that is being investigated. Thereby, we highlight the importance of the dFNC approach to investigate FNC. Given that the CHR group was predominantly antipsychotic-naive, it is also unlikely that observed patterns of dysconnectivity are due to medication effects.

Table 11. Summary of Significant Intrinsic Connectivity Network Pairs in States 1–5

ICN 1	*ICN 2*
Overview ICN pairs showing significant group effects in state 1	
Superior temporal gyrus R + L (AUD)	Postcentral gyrus R + L (SM)
Superior temporal gyrus R + L (AUD)	TPJ L (DMN)
Thalamus R + L (SC)	Superior temporal gyrus R + L (AUD)
SMA (SM)	Postcentral gyrus R (SM)
Postcentral gyrus R + L (SM)	Postcentral gyrus R (SM)
Postcentral gyrus R + L (SM)	TPJ L (DMN)
Supramarginal gyrus R + L (SM)	TPJ L (DMN)
TPJ L (DMN)	Cerebellum R + L (CB)
Overview ICN pairs showing significant group effects in state 2	
Superior temporal gyrus R + L (AUD)	Superior frontal gyrus medial (DMN)
Overview ICN pairs showing significant group effects in state 3	
Posterior parietal cortex R + L (CC)	Superior frontal gyrus medial (DMN)
Overview ICN pairs showing significant group effects in state 4	
Superior temporal gyrus R + L (AUD)	Postcentral gyrus R + L (SM)
Superior temporal gyrus R + L (AUD)	Superior frontal gyrus medial (DMN)
Superior temporal gyrus R + L (AUD)	TPJ L (DMN)
Thalamus R + L (SC)	Superior temporal gyrus R + L (AUD)
SMA (SM)	Postcentral gyrus R (SM)
Postcentral gyrus R + L (SM)	Postcentral gyrus R (SM)
Postcentral gyrus R + L (SM)	TPJ L (DMN)
Supramarginal gyrus R + L (SM)	TPJ L (DMN)
TPJ L (DMN)	Cerebellum R + L (CB)
Overview ICN pairs showing significant group effects in state 5	
Thalamus R + L (SC)	Superior temporal gyrus R + L (AUD)

Based on this study, future work could not only aim at providing longitudinal data but could also focus on specific regions previously shown to be implicated in predicting the transition from CHR to full-blown psychosis like the thalamus and other SC structures (Anticevic et al., 2015; Ferri et al., 2017).

Limitations

It is important to bear in mind that differences between ESZ and CHR groups may arise because all CHR individuals show attenuated forms of the same abnormalities evident in ESZ, or they may arise due to the admixture of the small subset of CHR individuals who will transition to psychosis, who may exhibit fully abnormal connectivity, with the large subset of CHR individuals who will not transition to psychosis, who may show little or no abnormalities in connectivity. At this point, our lack of sufficient follow-up data prevents the comparison of CHR converters and nonconverters needed to distinguish these possibilities.

Acknowledgments

This work was supported by National Institutes of Health grants 5P20RR021938/P20GM103472 (to V.D.C.), R01EB020407 (to V.D.C.), and R01MH076989 (to D.H.M.), and by National Science Foundation grant 1539067 (to V.D.C.). E.M. was funded by the Max Kade Foundation, New York City, New York, USA.

Author Disclosure Statement

No competing financial interests exist.

References

Abrol A, Damaraju E, Miller RL, Stephen JM, Claus ED, Mayer AR, Calhoun VD. 2017. Replicability of time-varying connectivity patterns in large resting state fMRI samples. Neuroimage 163:160–176.

Adams RA, Stephan KE, Brown HR, Frith CD, Friston KJ. 2013. The computational anatomy of psychosis. Front Psychiatry 4:47.

Alderson-Day B, McCarthy-Jones S, Fernyhough C. 2015. Hearing voices in the resting brain: a review of intrinsic functional connectivity research on auditory verbal hallucinations. Neurosci Biobehav Rev 55:78–87.

Allen EA, Damaraju E, Eichele T, Wu L, Calhoun VD. 2017. EEG signatures of dynamic functional network connectivity states. Brain Topogr 31:101–116.

Allen EA, Damaraju E, Plis SM, Erhardt EB, Eichele T, Calhoun VD. 2012. Tracking whole-brain connectivity dynamics in the resting state. Cereb Cortex 24:663–676.

Anticevic A, Cole MW, Repovs G, Murray JD, Brumbaugh MS, Winkler AM, et al. 2014. Characterizing thalamo-cortical disturbances in schizophrenia and bipolar illness. Cereb Cortex 24:3116–3130.

Anticevic A, Haut K, Murray JD, Repovs G, Yang GJ, Diehl C, et al. 2015. Association of thalamic dysconnectivity and conversion to psychosis in youth and young adults at elevated clinical risk. JAMA Psychiatry 72:882–891.

Arbabshirani MR, Kiehl KA, Pearlson GD, Calhoun VD. 2013. Classification of schizophrenia patients based on resting-state functional network connectivity. Front Neurosci 7:133.

Bell AJ, Sejnowski TJ. 1995. An information-maximization approach to blind separation and blind deconvolution. Neural Comput 7:1129–1159.

Calhoun VD, Adali T. 2012. Multisubject independent component analysis of fMRI: a decade of intrinsic networks, default

mode, and neurodiagnostic discovery. IEEE Rev Biomed Eng 5:60–73.

Calhoun VD, Adali T, Pearlson GD, Pekar JJ. 2001. A method for making group inferences from functional MRI data using independent component analysis. Hum Brain Mapp 14:140–151.

Calhoun VD, Eichele T, Pearlson GD. 2009. Functional brain networks in schizophrenia: a review. Front Hum Neurosci 3:17.

Calhoun VD, Miller RL, Pearlson GD, Adalı T. 2014. The chronnectome: time-varying connectivity networks as the next frontier in fMRI data discovery. Neuron 84:262–274.

Callaway DA, Perkins DO, Woods SW, Liu L, Addington J. 2014. Movement abnormalities predict transitioning to psychosis in individuals at clinical high risk for psychosis. Schizophr Res 159:263–266.

Camchong J, MacDonald AW, Bell C, Mueller BA, Lim KO. 2011. Altered functional and anatomical connectivity in schizophrenia. Schizophr Bull 37:640–650.

Cannon TD. 2015. How schizophrenia develops: cognitive and brain mechanisms underlying onset of psychosis. Trends Cogn Sci 19:744–756.

Cox RW. 1996. AFNI: software for analysis and visualization of functional magnetic resonance neuroimages. Comput Biomed Res 29:162–173.

Damaraju E, Allen EA, Belger A, Ford JM, McEwen S, Mathalon DH, et al. 2014. Dynamic functional connectivity analysis reveals transient states of dysconnectivity in schizophrenia. Neuroimage Clin 5:298–308.

Du Y, Fan Y. 2013. Group information guided ICA for fMRI data analysis. Neuroimage 69:157–197.

Du Y, Fryer SL, Fu Z, Lin D, Sui J, Chen J, et al. 2017a. Dynamic functional connectivity impairments in early schizophrenia and clinical high risk for psychosis. NeuroImage [Epub ahead of print]; DOI: 10.1016/j.neuroimage.2017.10.022.

Du Y, Fryer SL, Lin D, Sui J, Yu Q, Chen J, et al. 2017b. Identifying functional network changing patterns in individuals at clinical high risk for psychosis and patients with early illness schizophrenia: a group ICA study. Neuroimage Clin 17:335–346.

Du Y, Pearlson GD, Lin D, Sui J, Chen J, Salman M, et al. 2017c. Identifying dynamic functional connectivity biomarkers using GIG-ICA: application to schizophrenia, schizoaffective disorder, and psychotic bipolar disorder: identify dynamic connectivity states via GIG-ICA. Hum Brain Mapp 38:2683–2708.

Erhardt EB, Rachakonda S, Bedrick EJ, Allen EA, Adali T, Calhoun VD. 2011. Comparison of multi-subject ICA methods for analysis of fMRI data. Hum Brain Mapp 32: 2075–2095.

Ferri J, Fryer SL, Roach BJ, Loewy RL, Ford JM, Mathalon DH. 2017. Thalamic dysconnectivity in individuals at clinically high risk for schizophrenia and during early illness. Schizophr Bull 43:S44.

First MB, Spitzer RL, Gibbon M, Williams JBW. 2002. *Structured Clinical Interview for DSM-IV-TR Axis I Disorders, Research Version, Patient Edition*. New York: Biometrics Research, New York State Psychiatric Institute.

Forsyth JK, Lewis DA. 2017. Mapping the consequences of impaired synaptic plasticity in schizophrenia through development: an integrative model for diverse clinical features. Trends Cogn Sci 10:760–778.

Fox MD, Snyder AZ, Vincent JL, Corbetta M, Essen DCV, Raichle ME. 2005. The human brain is intrinsically organized into dynamic, anticorrelated functional networks. Proc Natl Acad Sci U S A 102:9673–9678.

Fusar-Poli P, Borgwardt S, Bechdolf A, Addington J, Riecher-Rössler A, Schultze-Lutter F, et al. 2013. The psychosis high-risk state: a comprehensive state-of-the-art review. JAMA Psychiatry 70:107–120.

Hasenkamp W, James GA, Boshoven W, Duncan E. 2011. Altered engagement of attention and default networks during target detection in schizophrenia. Schizophr Res 125: 169–173.

Himberg J, Hyvärinen A. Icasso: Software for Investigating the Reliability of ICA Estimates by Clustering and Visualization. In Neural Networks for Signal Processing, 2003. NNSP'03 IEEE 13th workshop, Toulouse, France, 2003, pp. 259–268.

Jafri MJ, Pearlson GD, Stevens M, Calhoun VD. 2008. A method for functional network connectivity among spatially independent resting-state components in schizophrenia. Neuroimage 39:1666–1681.

Jardri R, Pouchet A, Pins D, Thomas P. 2011. Cortical activations during auditory verbal hallucinations in schizophrenia: a coordinate-based meta-analysis. JAMA Psychiatry 168:73–81.

Kaufman J, Birmaher B, Brent D, Rao U, Flynn C, Moreci P, et al. 1997. Schedule for affective disorders and schizophrenia for school-age children-present and lifetime version (K-SADS-PL): initial reliability and validity data. J Am Acad Child Adolesc Psychiatry 36:980–988.

Kay SR, Flszbein A, Opfer LA. 1987. The positive and negative syndrome scale (PANSS) for schizophrenia. Schizophr Bull 13:261:276.

Ma S, Correa NM, Li XL, Eichele T, Calhoun VD, Adali T. 2011. Automatic identification of functional clusters in fMRI data using spatial dependence. IEEE Trans Biomed Eng 58:3406–3417.

Manoliu A, Riedl V, Zherdin A, Mühlau M, Schwerthöffer D, Scherr M, et al. 2014. Aberrant dependence of default mode/central executive network interactions on anterior insular salience network activity in schizophrenia. Schizophr Bull 40:428–437.

McGlashan TH, Miller TJ, Woods SW, Hoffman RE, Davidson L. 2001. Instrument for the assessment of prodromal symptoms and states. In: Miller T, Mednick SA, McGlashan TH, Libiger J, Johannessen JO (eds.) *Early Intervention in Psychotic Disorders*. Dordrecht, Netherlands: Springer; pp. 135–149.

McKeown MJ, Makeig S, Brown GG, Jung TP, Kindermann SS, Bell AJ, Sejnowski, TJ. 1998. Analysis of fMRI data by blind separation into independent spatial components. Hum Brain Mapp 6:160–188.

Miller TJ, McGlashan TH, Rosen JL, Cadenhead K, Ventura J, McFarlane W, et al. 2003. Prodromal assessment with the structured interview for prodromal syndromes and the scale of prodromal symptoms: predictive validity, interrater reliability, and training to reliability. Schizophr Bull 29:703–715.

Miller TJ, McGlashan TH, Rosen JL, Somjee L, Markovich PJ, Stein K, Woods SW. 2002. Prospective diagnosis of the initial prodrome for schizophrenia based on the structured interview for prodromal syndromes: preliminary evidence of interrater reliability and predictive validity. JAMA Psychiatry 159:863–865.

Phillips LJ, McGorry PD, Yung AR, McGlashan TH, Cornblatt B, Klosterkötter J. 2005. Prepsychotic phase of schizophrenia and related disorders: recent progress and future opportunities. Br J Psychiatry 187:s33–s44.

Power JD, Mitra A, Laumann TO, Snyder AZ, Schlaggar BL, Petersen SE. 2014. Methods to detect, characterize, and remove motion artifact in resting state fMRI. Neuroimage 84:320–341.

Rashid B, Damaraju E, Pearlson GD, Calhoun VD. 2014. Dynamic connectivity states estimated from resting fMRI Identify differences among schizophrenia, bipolar disorder, and healthy control subjects. Front Hum Neurosci 8:897.

Roweis S. 1998. EM algorithms for PCA and SPCA. In: Kearns MJ, Solla SA, Cohn DA (eds.) *Advances in Neural Information Processing Systems.* Cambridge, Massachusetts: MIT Press; pp. 626–632.

Rubinov M, Bullmore E. 2013. Schizophrenia and abnormal brain network hubs. Dialogues Clin Neurosci 15:339–349.

Shim G, Oh JS, Jung WH, Jang JH, Choi CH, Kim E, et al. 2010. Altered resting-state connectivity in subjects at ultra-high risk for psychosis: an fMRI study. Behav Brain Funct 6:58.

Shine JM, Bissett PG, Bell PT, Koyejo O, Balsters JH, Gorgolewski KJ, et al. 2016. The dynamics of functional brain networks: integrated network states during cognitive task performance. Neuron 92:544–554.

Thoma RJ, Chaze C, Lewine JD, Calhoun VD, Clark VP, Bustillo J, et al. 2016. Functional MRI evaluation of multiple neural networks underlying auditory verbal hallucinations in schizophrenia spectrum disorders. Front Psychiatry 7:39.

Tzourio-Mazoyer N, Landeau B, Papathanassiou D, Crivello F, Etard O, Delcroix N, et al. 2002. Automated anatomical labeling of activations in SPM Using a macroscopic anatomical parcellation of the MNI MRI single-subject brain. Neuroimage 15:273–289.

Van Harten PN, Walter S, Kent JS, Sponheim SR, Mittal VA. 2017. The clinical and prognostic value of motor abnormalities in psychosis, and the importance of instrumental assessment. Neurosci Biobehav Rev 80:476–487.

Vatansever D, Menon DK, Manktelow AE, Sahakian BJ, Stamatakis EA. 2015. Default mode dynamics for global functional integration. J Neurosci 35:15254–15262.

Vercammen A, Knegtering H, den Boer JA, Liemburg EJ, Aleman A. 2010. Auditory hallucinations in schizophrenia are associated with reduced functional connectivity of the temporo-parietal area. Biol Psychiatry 67:912–918.

Whitfield-Gabrieli S, Ford JM. 2012. Default mode network activity and connectivity in psychopathology. Annu Rev Clin Psychol 8:49–76.

Whitfield-Gabrieli S, Thermenos HW, Milanovic S, Tsuang MT, Faraone SV, McCarley RW, et al. 2009. Hyperactivity and hyperconnectivity of the default network in schizophrenia and in first-degree relatives of persons with schizophrenia. Proc Natl Acad Sci U S A 106:1279–1284.

Woodward ND, Karbasforoushan H, Heckers S. 2012. Thalamocortical dysconnectivity in schizophrenia. JAMA Psychiatry 169:1092–1099.

Wotruba D, Michels L, Buechler R, Metzler S, Theodoridou A, Gerstenberg M, et al. 2013. Aberrant coupling within and across the default mode, task-positive, and salience network in subjects at risk for psychosis. Schizophr Bull 40:1095:1104.

Yan CG, Zang Y. 2010. DPARSF: a MATLAB toolbox for ''Pipeline'' data analysis of resting-state fMRI. Front Syst Neurosci 4:13.

Address correspondence to:
Vince D. Calhoun
The Mind Research Network
1101 Yale Boulevard NE
Albuquerque, NM 87131

E-mail: vcalhoun@mrn.org

Daniel H. Mathalon
Mental Health Service
San Francisco VA Medical Center/Psychiatry Service (116D)
4150 Clement Street
San Francisco, CA 94121

E-mail: daniel.mathalon@ucsf.edu